

Floquet spectrum for anisotropic and tilted Dirac materials under linearly polarized light at all field intensities

J. C. Sandoval-Santana,^{1, a)} V. G. Ibarra-Sierra,^{2, b)} A. Kunold,^{3, c)} and Gerardo G. Naumis^{2, d)}

¹⁾*Instituto de Física, Universidad Nacional Autónoma de México, Apartado Postal 20-364 01000, Ciudad de México, México*

²⁾*Departamento de Sistemas Complejos, Instituto de Física, Universidad Nacional Autónoma de México, Apartado Postal 20-364, 01000, Ciudad de México, México.*

³⁾*Área de Física Teórica y Materia Condensada, Universidad Autónoma Metropolitana Azcapotzalco, Av. San Pablo 180, Col. Reynosa-Tamaulipas, 02200 Ciudad de México, México*

(Dated: 30 March 2020)

The Floquet spectrum in an anisotropic tilted Dirac semimetal modulated by linearly polarized light is addressed through the solution of the time-dependent Schrödinger equation for the two-dimensional Dirac Hamiltonian via the Floquet theorem. The time-dependent wave functions and the quasienergy spectrum of the two-dimensional Dirac Hamiltonian under the normal incidence of linearly polarized waves are obtained for an arbitrarily intense electromagnetic radiation. We applied a set of unitary transformations to reduce the Schrödinger equation to an ordinary second-order differential Hill equation with complex coefficients. Through the stability analysis of this differential equation, the weak and strong field regimes are clearly distinguished in the quasi-spectrum. In the weak electric field regime, above a certain threshold given by the field parameters, the spectrum mostly resembles that of free electrons in graphene. Below this threshold, in the strong electric field regime, the spectrum abruptly becomes highly anisotropic and a gap opens up. As an example, we apply the results to the particular case of borophene.

I. INTRODUCTION

The superior physical, mechanical and chemical properties of two-dimensional (2D) materials makes them an ideal playground to study new and exciting kinds of quantum phases¹⁻⁷. Their remarkable electronic and optical features have intensely driven the development of novel and innovative optoelectronic devices⁸⁻¹⁰ as broad band optical modulators¹¹⁻¹³, solar cells^{14,15}, infrared photodetectors¹⁶ and hybrid plasmonic devices^{17,18}.

In the last decade persistent efforts have been made to harness the unique features of graphene's so-called dressed electrons^{8,16,19-27} to design different kinds of optoelectronic devices. Electromagnetic dressing, attained when electrons strongly couple to electromagnetic fields, substantially renormalize the energy and the velocities in graphene²⁷. In turn, renormalized parameters highly depend on the light polarization: in graphene circularly polarized fields open a dynamical gap in the Dirac point while linearly polarized fields live it intact. Particularly, dressed electrons under linearly polarized light induce an anisotropy of the electron dispersion relation²⁶. Electromagnetic dressing could, therefore, be used to tune the electronic and optical properties of graphene, including band gap and carrier velocities²⁷ which are clearly manifest in several measurable physical properties as the photocurrent^{23,28}. A similar approach has been adopted in ultrafast material science promising optical and mechanical control of the physical properties of 2D materials²⁹. In this case, it is time-dependent strain that acts as pseudo-electromagnetic field³⁰.

In graphene, the weak-field regime, where light-matter coupling is perturbative³¹⁻³³, is well understood. It may be pictured as a quantized-photon field interacting with massless Dirac fermions having a conic dispersion relation. However, in the intense-field regime, this perturbative expansion cannot converge. The Dirac dispersion relation is highly distorted as a result of the electronic dressing rendering the quantized-photon picture invalid. It is clear then that this emerging field requires new theoretical tools that go beyond the conventional techniques^{34,35}. There are numerous proposals to approach this problem^{19-22,24-26}, but, even for graphene, some aspects of the interaction between carriers and strong time-driven fields remain elusive.

Another essential question that remains to be fully answered is how such an intense electromagnetic radiation would affect other Dirac materials^{36,37} as borophene or black-phosphorus³⁸⁻⁴¹, for example. Particularly borophene is a remarkable anisotropic material^{2,6,42,43}. After being theoretically predicted thirty years ago⁴⁴, it was until 2015 that it was synthesized⁴⁵. Borophene turns out to be stronger and even more flexible than graphene. It is a good conductor of both electricity and heat and it is expected to be a superconductor⁴⁶ with relatively high transition temperatures.

In a series of recent papers, we have investigated time-driven anisotropic Dirac Hamiltonians as the one that describes borophene^{42,43,47,48}. However, the mathematical complexity of the problem required several approximations that are only valid for very intense fields^{43,48}. Therefore, the critical link between weak fields, treatable with perturbation theory, and strong fields is still missing. In particular, the cases of linearly and elliptically polarized light were studied in the intense field regime^{43,48}, where the rather convoluted Hill equation with time dependent coefficients was simplified into the very well known Mathieu equation with constant coefficients. Nevertheless, the complete study of the Hill equation entails the interplay between the strong and weak field intensity

^{a)}Electronic mail: jcarlooss@fisica.unam.mx

^{b)}Electronic mail: vickkun@fisica.unam.mx

^{c)}Electronic mail: akb@azc.uam.mx

^{d)}Electronic mail: naumis@fisica.unam.mx

regimes, key to comprehend the formation of the quasienergy spectrum. This effect can be thoroughly studied by analyzing the quasi-energy spectrum using the Floquet theory^{49–53}.

In this paper we address the general problem of a particle that obeys the anisotropic Dirac Hamiltonian subject to linearly polarized light with an arbitrarily large field intensity. The calculation of the quasienergy spectrum and the wave function is achieved through a set of unitary transformations that enables to reduce the matrix differential equation into a scalar differential equation. This, in turn, is readily solved via the Floquet theorem and a Fourier spectral decomposition of the periodical part of the solution. It is shown that in the intense field regime the quasienergy spectrum abruptly develops an anisotropic structure, absent in the weak field regime.

The paper is organized as follows. In Sec. II we introduce the low-energy effective two-dimensional anisotropic Dirac Hamiltonian and we study the case of borophene subject to an arbitrarily intense linearly polarized electromagnetic field. Subsequently, in Sec. III, we analyze the quasienergy spectrum that emerges from the Hill equation by means of the Floquet approach. Also, we find the time-dependent wave functions. Finally, we summarize and conclude in Sec. IV.

II. TWO-DIMENSIONAL ELECTRONS IN A TILTED DIRAC CONE SUBJECT TO ELECTROMAGNETIC FIELDS

A. The anisotropic Dirac Hamiltonian

We start by considering a low-energy anisotropic Dirac Hamiltonian close to one of the Dirac points. In the particular case of 8 – $Pmmn$ borophene it is given by^{42,43,47,54}

$$\hat{H} = \hbar v_t k_y \hat{\sigma}_0 + \hbar [v_x k_x \hat{\sigma}_x + v_y k_y \hat{\sigma}_y], \quad (1)$$

where k_x and k_y are the components of the two-dimensional momentum vector \mathbf{k} , $\hat{\sigma}_x$ and $\hat{\sigma}_y$ are the Pauli matrices, and $\hat{\sigma}_0$ is the 2×2 identity matrix. The three velocities in the anisotropic 8 – $Pmmn$ borophene Dirac Hamiltonian (1) are given by $v_x = 0.86v_F$, $v_y = 0.69v_F$ and $v_t = 0.32v_F$ where $v_F = 10^6 \text{ m/s}$ ⁴⁷ is the Fermi velocity. In Eq. (1), the last two terms give rise to the familiar form of the kinetic energy leading to the Dirac cone and the first one tilts the Dirac cone in the k_y direction. These two features are contained in the energy dispersion relation⁴⁸

$$E_{\eta,k} = \left(\frac{v_t}{v_y} \right) \tilde{k}_y + v \varepsilon, \quad (2)$$

where

$$\varepsilon = \sqrt{\tilde{k}_x^2 + \tilde{k}_y^2}, \quad (3)$$

and $v = \pm 1$ is the band index. In Eq. (2), we used the set of renormalized moments $\tilde{k}_x = \hbar v_x k_x$, $\tilde{k}_y = \hbar v_y k_y$. The corresponding free electron wave function is,

$$\psi_v(\mathbf{k}) = \frac{1}{\sqrt{2}} \begin{bmatrix} 1 \\ v \exp(i\theta_k) \end{bmatrix} \quad (4)$$

where $\theta_k = \tan^{-1}(\tilde{k}_y/\tilde{k}_x)$.

B. Linearly polarized waves

Now we consider a charge carrier, described by the two-dimensional anisotropic Dirac Hamiltonian, subject to an electromagnetic wave that propagates along a direction perpendicular to the surface of the crystal. The effects of the electromagnetic field are introduced in the Hamiltonian (1) through the Peierls substitution⁵⁵ $\hbar \mathbf{k} \rightarrow \hbar \mathbf{k} - e\mathbf{A}$ where $\mathbf{A} = (A_x, A_y)$ is the vector potential of the electromagnetic wave. A considerable simplification can be achieved by adopting a gauge in which \mathbf{A} only depends on time. The Hamiltonian (1) is thus transformed into

$$\hat{H} = \frac{v_t}{v_y} (\tilde{k}_y - ev_y A_y) \hat{\sigma}_0 + (\tilde{k}_x - ev_x A_x) \hat{\sigma}_x + (\tilde{k}_y - ev_y A_y) \hat{\sigma}_y. \quad (5)$$

Assuming that the electromagnetic wave is linearly polarized, the vector potential can be written as

$$\mathbf{A} = \frac{E_0}{\Omega} \cos(\Omega t) \hat{\mathbf{r}}, \quad (6)$$

where $\hat{\mathbf{r}} = (1, 0)$ is the polarization vector, E_0 is the uniform amplitude of the electric field and Ω is the angular frequency of the electromagnetic wave. Observe that here the field \mathbf{A} is not quantized and is treated classically. Thus, our results are valid for a field with a large number of photons, which can be represented by a quantum coherent field. In the Schrödinger equation corresponding to (5),

$$i\hbar \frac{d}{dt} \Psi(t) = \hat{H} \Psi(t), \quad (7)$$

the two dimensional spinor can be expressed as $\Psi(t) = (\Psi_A(t), \Psi_B(t))^\top$, where A and B label the two sublattices.

The main difficulty in deducing the wave function's explicit form resides in that the Hamiltonian (5) couples the differential equations for the $\Psi_A(t)$ and $\Psi_B(t)$ spinor components due to the terms that are proportional to $\hat{\sigma}_x$ and $\hat{\sigma}_y$. To uncouple the spinor components we proceed as follows. First, applying a 45° rotation around the k_y axis of the form

$$\Psi(t) = \exp \left[-\frac{i}{\hbar} \left(\frac{\pi}{4} \right) \hat{\sigma}_y \right] \Phi(t), \quad (8)$$

conveniently transforms the non-diagonal $\hat{\sigma}_x$ matrix into $\hat{\sigma}_z$. Indeed, substituting (8) into Eq. (7) yields

$$i \frac{d}{d\phi} \Phi(\phi) = \frac{2}{\hbar \Omega} \left[\left(\frac{v_t}{v_y} \right) \tilde{k}_y \hat{\sigma}_0 + \tilde{\Pi}_x \hat{\sigma}_z + \tilde{k}_y \hat{\sigma}_y \right] \Phi(\phi), \quad (9)$$

where the only non-diagonal remaining term is the one proportional to $\hat{\sigma}_y$. In the foregoing equation, $\phi = \Omega t/2$, $\tilde{\Pi}_x = \tilde{k}_x - \zeta_x \cos(2\phi)$ and $\zeta_x = ev_x E_x/\Omega$. The spinor components of $\Phi(\phi) = (\Phi_+(\phi), \Phi_-(\phi))^\top$ are given by $\Phi_+(\phi) = [\Psi_A(\phi) + \Psi_B(\phi)]/\sqrt{2}$ and $\Phi_-(\phi) = [\Psi_A(\phi) - \Psi_B(\phi)]/\sqrt{2}$. Second, the term proportional to $\hat{\sigma}_0$ in Eq. (9) is removed by adding a time-dependent phase to the wave function

$$\Phi(\phi) = \exp \left[-2i \left(\frac{v_t}{v_y} \right) \frac{\tilde{k}_y}{\hbar \Omega} \phi \hat{\sigma}_0 \right] \chi(\phi), \quad (10)$$

where $\chi(\phi) = (\chi_{+1}(\phi), \chi_{-1}(\phi))^T$. Finally, after inserting Eq. (10) into Eq. (9), we follow the procedure shown in Appendix A. The resulting differential equation takes on the form of the Hill equation⁵⁶

$$\chi''(\phi) + \mathbb{F}(\phi)\chi(\phi) = 0, \quad (11)$$

where the matrix $\mathbb{F}(\phi)$ is defined as

$$\mathbb{F}(\phi) = [a + q_1 \cos(2\phi) + q_2 \cos(4\phi)] \hat{\sigma}_0 + q_3 \sin(2\phi) \hat{\sigma}_z. \quad (12)$$

The Hill equation parameters

$$a = \left(\frac{2}{\hbar\Omega}\right)^2 \left(\varepsilon^2 + \frac{\zeta_x^2}{2}\right), \quad (13)$$

$$q_1 = -8 \left(\frac{\tilde{k}_x}{\hbar\Omega}\right) \left(\frac{\zeta_x}{\hbar\Omega}\right), \quad (14)$$

$$q_2 = 2 \left(\frac{\zeta_x}{\hbar\Omega}\right)^2, \quad (15)$$

$$q_3 = 4i \left(\frac{\zeta_x}{\hbar\Omega}\right). \quad (16)$$

are expressed in terms of the ratios of the characteristic energies of the system. Thereby, $\varepsilon/\hbar\Omega$ is the ratio of the electron kinetic energy to the photon energy, $\zeta_x/\hbar\Omega$ is the ratio of the work done on the charged carries by the electromagnetic wave to the photon energy and $\tilde{k}_x/\hbar\Omega$ is the ratio of the x part of the electron kinetic energy to the photon energy.

Expressing (11) as a second order differential equation is quite advantageous for the calculations that follow. First, the evolution operator that propagates the state χ in time must be diagonal since $\mathbb{F}(\phi)$ is solely composed of the diagonal matrices $\hat{\sigma}_0$ and $\hat{\sigma}_z$. As a consequence of this, the scalar differential equations for the $\chi_{+1}(\phi)$ and $\chi_{-1}(\phi)$ spinor components decouple. Moreover, the differential equation for the $\chi_{-1}(\phi)$ component turns out to be the complex conjugate of the one for $\chi_{+1}(\phi)$. Both differential equations may be summarized by

$$\chi''_{\eta}(\phi) + [a + q_1 \cos(2\phi) + q_2 \cos(4\phi) + \eta q_3 \sin(2\phi)] \chi_{\eta}(\phi) = 0, \quad (17)$$

where $\eta = \pm 1$.

This alternative form of the Schrödinger equation considerably simplifies the computation and analysis of the stability spectrum.

III. QUASIENERGY SPECTRUM AND WAVE FUNCTION

A. Quasienergy spectrum

In this section, we analyse the quasienergy spectrum produced by the Hill equation (17), and its relations with the stability of its solutions. The determination of the stability regions of this differential equation is quite challenging mainly

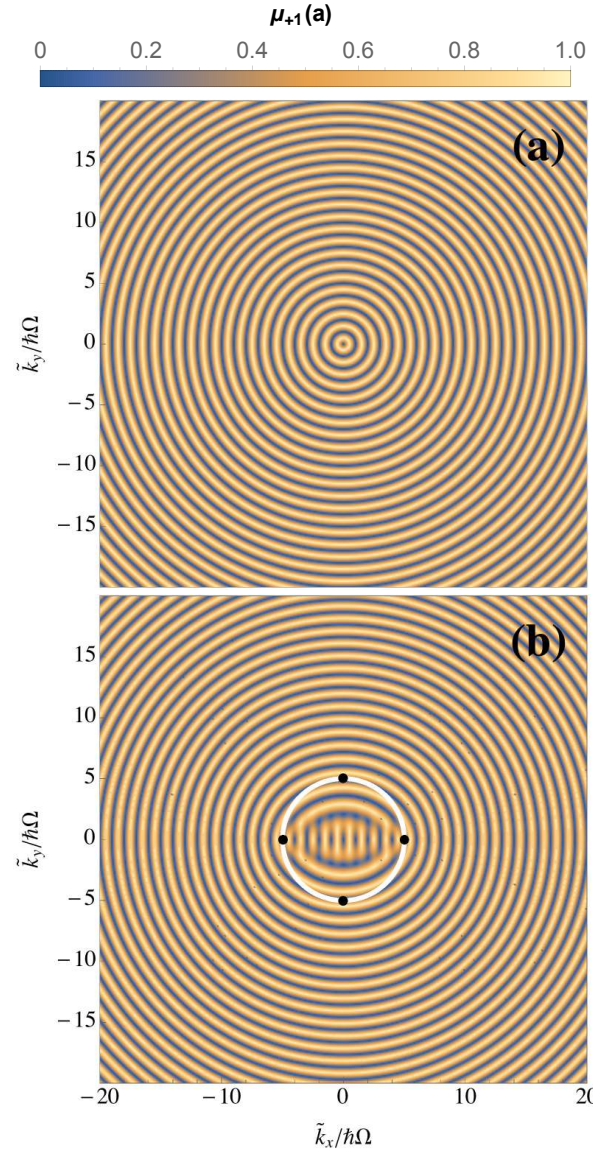


FIG. 1. Density plot of the characteristic exponent spectrum $\mu_{+1}(a)$ as a function of $\tilde{k}_x/\hbar\Omega$ and $\tilde{k}_y/\hbar\Omega$ for (a) $\zeta_x/\hbar\Omega = 10^{-3}$ with $E_x = 10^{-4}$ V/m and (b) $\zeta_x/\hbar\Omega = 5$ with $E_x = 9.7$ V/m. In both cases the frequency of the electromagnetic field has a value $\Omega = 50 \times 10^9$ Hz. The white circle indicates the theoretical threshold given by the radius $\varepsilon = \zeta_x$ at which there is a transition from field-driven strong to weak anisotropy solution. The black dots denote the limits of the white circle in the cases where $\tilde{k}_x/\hbar\Omega = 0$ and $\tilde{k}_y/\hbar\Omega = 0$.

due to the imaginary coefficient q_3 . The real coefficients a , q_1 and q_2 alone give rise to the Whittaker-Hill equation⁵⁷, widely discussed in the spectral theory of periodic differential equations. The imaginary coefficient q_3 , however, introduces additional difficulties that are rarely addressed in the literature⁵⁸. Among other things, it yields complex characteristic values. Despite the added complexity, Eq. (17) may be approached by Whittaker's original assumption^{56,59} that the solution should take the Floquet normal form

$$\chi_{\eta}(\phi) = \exp[i\mu_{\eta}\phi] u_{\eta}(\phi), \quad (18)$$

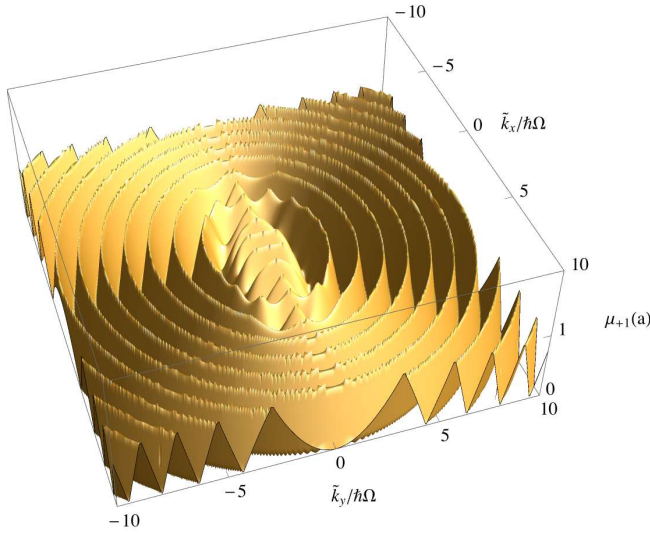


FIG. 2. Characteristic exponent spectrum $\mu_{+1}(a)$ as a function of the normalized momenta $\tilde{k}_x/\hbar\Omega$ and $\tilde{k}_y/\hbar\Omega$. This plot was made for $\zeta_x/\hbar\Omega = 5$ with $E_x = 9.7$ V/m and $\Omega = 50 \times 10^9$ Hz.

due to the periodicity of the Hamiltonian. Also, according to the Floquet theorem, $u_\eta(\phi)$ must be a function with period π . The function $\mu_\eta(a)$ is termed the characteristic exponent. As detailed in the following sections, the characteristic exponent and the quasienergy spectrum are closely connected. Thanks to the periodicity of the $u_\eta(\phi)$ function, $\chi_\mu(\phi)$ might be expressed as a Fourier series expansion. In this manner, the second-order differential equation with time-variable periodic coefficients is traded for a matrix eigenvalue problem. The eigenvalues that stem from it are precisely the characteristic exponents $\mu_\eta(a)$. These have the form

$$\mu_\eta(a) = \frac{1}{\pi} \cos^{-1} [1 + \Delta_\eta(0) (\cos(\sqrt{a}\pi) - 1)], \quad (19)$$

where a and $\Delta_\eta(0)$ are given by Eqs. (13) and (A9), respectively. For a detailed calculation of $\mu_\eta(a)$ refer to Appendix A.

In general, the solutions of the Hill equation (17) fall either on stable ($\text{Im}[\mu_\eta(a)] = 0$) or unstable regions ($\text{Im}[\mu_\eta(a)] \neq 0$) depending on the values taken by the coefficients a , q_1 , q_2 and q_3 ^{57–59}. Surprisingly, the solutions mostly fall on the stable regions when these coefficients are restricted by the parametrization of Eqs. (13)–(16) for seemingly arbitrary domain spaces of \tilde{k}_x , \tilde{k}_y and ζ_x . Fig. 1 shows a density plot of the characteristic exponent spectrum for $\mu_{+1}(a)$ as a function of the normalized momenta $\tilde{k}_x/\hbar\Omega$ and $\tilde{k}_y/\hbar\Omega$. Over the entire parameter space covered in this figure the solutions of the Hill equation are stable.

One of most striking features of the spectrum emerges when one compares the quasienergies at low and high electric field amplitudes. The contrast between the effects of weak ($E_x = 10^{-4}$ V/m, $\zeta_x/\hbar\Omega = 10^{-3}$) and strong ($E_x = 9.7$ V/m, $\zeta_x/\hbar\Omega = 5$) electric field amplitudes is shown in Figs. 1 (a) and (b) respectively. In the weak electric field regime (see Fig. 1 (a)) the isolines of the characteristic exponent $\mu_{+1}(a)$ as a

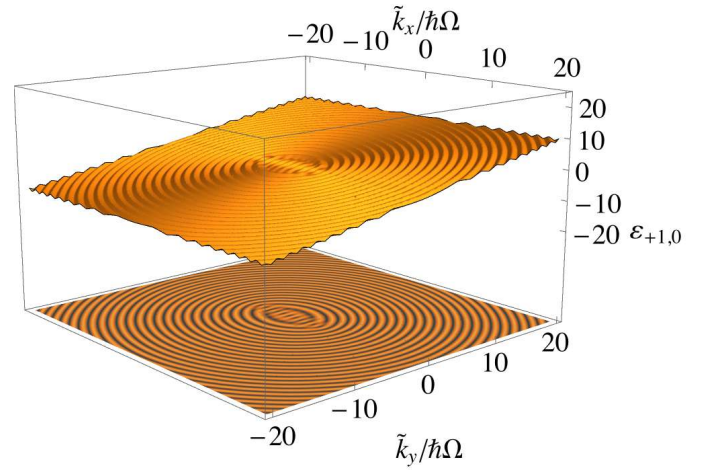


FIG. 3. Quasienergy $\mathcal{E}_{+1,0}$ spectrum as a function of the normalized momenta $\tilde{k}_x/\hbar\Omega$ and $\tilde{k}_y/\hbar\Omega$ in the strong electric field regime ($\zeta_x/\hbar\Omega = 5$, $E_x = 9.7$ V/m) for $\Omega = 50 \times 10^9$ Hz. The density plot at the bottom of the plot is a projection of the 3D plot at the top. 1(b).

function of the normalized momenta form a pattern of concentric circles. In the strong electric field regime (see Fig. 1 (b)) a spectrum of vertical lines, perpendicular to the electric field direction, emerges close to the Dirac point ($\tilde{k}_x = \tilde{k}_y = 0$). The vertical grill is surrounded by an elliptical outline that is approximately delimited by the white circle of radius $\varepsilon = \zeta_x$. In the vicinity of this contour ($\varepsilon > \zeta_x$) the spectrum takes on an elliptical form but further out ($\varepsilon \gg \zeta_x$) the spectrum recovers the circular shape observed in the low electric field regime.

The appearance of the vertical grill in the quasienergy spectrum is due to the interplay between the terms $\cos(2\phi)$, $\sin(2\phi)$ and $\cos(4\phi)$ in Eq. (17). For example, $\varepsilon < \zeta_x$ implies that $q_2 > |q_3|$ and $|q_3| > q_1$, therefore the most significant term is $\cos(4\phi)$. By contrast, $\varepsilon > \zeta_x$ implies that $q_1 > |q_3|$ and $|q_3| > q_1$, and the dominant element is $\cos(2\phi)$.

Further details of the spectrum are appreciated in Fig. 2 where we show a 3D plot of the quasienergy $\mu_{+1}(a)$ as a function of \tilde{k}_x and \tilde{k}_y in the high electric field regime ($\zeta_x/\hbar\Omega = 5$).

B. Wave function and Floquet spectrum

As mentioned above, the wave function in (7) must satisfy the Floquet theorem as a result of the time periodicity of the Hamiltonian (5). Hence, following the Floquet theorem, Eqs. (8), (10) and (18) can be combined into the wave function

$$\Psi(\phi) = \mathcal{N} \exp \left[-\frac{i}{\hbar} \left(\frac{\pi}{4} \right) \hat{\sigma}_y \right] \mathcal{U}(\phi) \chi(0), \quad (20)$$

where \mathcal{N} is a normalization constant, $\chi(0) = (\chi_{+1}(0), \chi_{-1}(0))^\top$ is the initial state vector in (17) and $\mathcal{U}(\phi)$ denotes the time evolution operator such that $\chi(\phi) = \mathcal{U}(\phi) \chi(0)$. As we pointed out before, because $\mathbb{F}(\phi)$ is a diagonal matrix, the evolution operator must also be

diagonal. Thus, it can be expressed quite generally as

$$\mathcal{U}(\phi) = \begin{pmatrix} \exp[-i\varepsilon_{+1}\phi]u_{+1}(\phi) & 0 \\ 0 & \exp[-i\varepsilon_{-1}\phi]u_{-1}(\phi) \end{pmatrix}, \quad (21)$$

where $u_{-1}(\phi) = u_{+1}^*(\phi)$ have period π and

$$\varepsilon_\eta = 2\frac{v_x}{v_y}\frac{\tilde{k}_y}{\hbar\Omega} + \mu_\eta(a). \quad (22)$$

It is easy to verify that the wave function (20) reduces to the free-particle wave function (4) when the electric field vanishes. From the Floquet theory^{60–63}, the time evolution operator is periodic $\mathcal{U}(\phi) = \mathcal{U}(\phi + l\pi)$ and quasienergy can be expressed as

$$\mathcal{E}_{\eta,l} = \varepsilon_\eta + l = 2\frac{v_x}{v_y}\frac{\tilde{k}_y}{\hbar\Omega} + \mu_{\eta,l}(a), \quad (23)$$

where

$$\mu_{\eta,l}(a) = \mu_\eta(a) + l, \quad l \in \mathbb{Z}, \quad (24)$$

is the characteristic exponent for different Brillouin zones which are tagged by the integer subscript l .

In Fig. 3, we show the quasienergy for $\mathcal{E}_{+1,0}$. At the bottom of this figure, a density plot of $\mu_{+1,0}(a)$ is shown for reference. One notes that the spectrum consists of the quasienergies $\mu_{+1}(a)$, plotted in Fig. 2, on to the tilt that comes from the first term of Eq. (23). It arises from the anisotropic character of the Hamiltonian (1). Even though it strongly distorts the symmetry of the Dirac cone, it has been shown that interband transitions are not affected by it in the zero-temperature limit⁵⁴.

Different cross sections of the quasienergy spectrum $\mu_{\eta,l}(a)$ are shown in Fig. 4 for the Brillouin zones $l = -1, 0, 1$. Panels (a) and (b) show the spectrum section planes $\tilde{k}_y = 0$ and $\tilde{k}_x = 0$, respectively, in the weak electric field regime ($\zeta_x/\hbar\Omega = 10^{-3}$, $E_x = 10^{-3}$ V/m, and $\Omega = 50 \times 10^9$ Hz). In this case, both $\tilde{k}_y = 0$ and $\tilde{k}_x = 0$ cross sections are almost identical since the electric field is not intense enough to provoke any distortion to the free particle spectrum. The quasienergies for the many Brillouin zones as functions of \tilde{k}_x [panel (a)] or \tilde{k}_y [panel (b)] have the form of a triangular function. In the strong electric field regime ($\zeta_x/\hbar\Omega = 5$, $E_x = 9.7$ V/m and $\Omega = 50 \times 10^9$ Hz) both cuts are radically different. In panel (c) we note that the $\tilde{k}_y = 0$ cross section of the spectrum resembles those corresponding to the weak electric field regime also exhibiting a triangular shaped function of \tilde{k}_x . However, in the $\tilde{k}_x = 0$ plane [panel (d)] the presence of the electromagnetic field becomes evident as the spectrum is warped approximately in the domain $-2 < \tilde{k}_y < 2$. At both ends of this range the quasienergy abruptly recovers the triangular feature that characterizes the spectrum in the absence of electromagnetic radiation. This distortion is roughly bounded by the two black vertical lines that correspond to the black dots in Fig. 1 (b), where the strength of the electromagnetic field is comparable to the energy of the unperturbed system, i.e. $\varepsilon = \zeta_x$.

A quite robust feature of the spectrum is the preservation of the gapless Dirac cone in the vicinity of the Dirac point: the

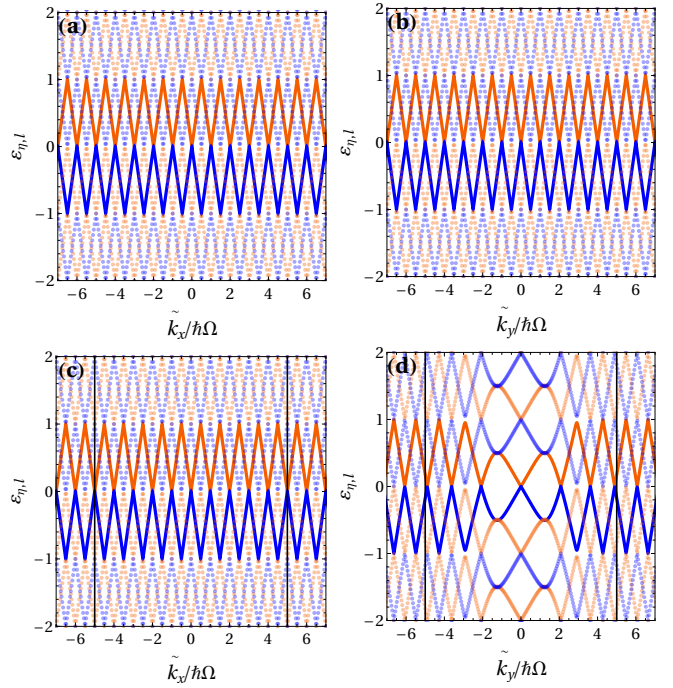


FIG. 4. Section planes of the quasienergy $\mu_{\eta,l}(a)$ as a function of $\tilde{k}_x/\hbar\Omega$ or $\tilde{k}_y/\hbar\Omega$ for the Brillouin zones $l = -1, 0, 1$. Panels (a) and (b) correspond to the weak electric field regime ($\zeta_x/\hbar\Omega = 10^{-3}$, $E_x = 10^{-3}$ V/m, and $\Omega = 50 \times 10^9$ Hz). The strong electric field regime ($\zeta_x/\hbar\Omega = 5$, $E_x = 9.7$ V/m and $\Omega = 50 \times 10^9$ Hz) is shown in panels (c) and (d). The solid orange and blue lines correspond to the quasienergies $\mu_{+1,0}(a)$ and $\mu_{-1,0}(a)$, respectively. The light dots plot the quasienergy $\mu_{\pm 1, \pm 1}(a)$ in the adjacent Brillouin zones ($l = \pm 1$). The threshold $\varepsilon = \zeta_x$, where the energy of the electric field ζ_x is identical to the unperturbed energy ε , is indicated by the vertical black lines in panels (c) and (d).

quasienergies $\mu_{+1,l}$ and $\mu_{-1,l}$ as well as $\mathcal{E}_{+1,l}$ and $\mathcal{E}_{-1,l}$ touch at the tip of the Dirac point despite the intensity of the linearly polarized electromagnetic field. Nevertheless, the conic dispersion relation is stretched along the k_y direction as a result of the renormalization of the v_y component of the velocity due to electronic dressing. Despite the absolute absence of a gap at the tip of the Dirac cone, it is possible to open up gaps in other zones of the spectrum. In Fig. 4 (d), the appearance of a small gap between $\mu_{+1,l}$ and $\mu_{-1,l}$ can be appreciated at $\tilde{k}_y/\hbar\Omega \approx \pm 2$.

IV. CONCLUSIONS

We investigated the quasienergy spectrum of an anisotropic tilted Dirac material subject to an arbitrarily intense linearly polarized electromagnetic field. To this end, we studied the behavior of 8-*Pmmn* borophene under the normal incidence of a linearly polarized field. We worked out the time-dependent wave function and the quasienergy spectrum from the Schöendinger equation via the Floquet theory. The quasienergy spectrum exhibits a sharp difference between the

weak and strong electromagnetic field regimes. While in the first the quasienergy as a function of the quasimomenta (\tilde{k}_x and \tilde{k}_y) is highly isotropic the latter presents an anisotropic pattern in the low energy region that resembles a grid aligned perpendicularly to the direction of the radiation's electric field. This pattern abruptly disappears beyond the threshold where the free kinetic energy of the carriers is larger than the energy associated to the electric field. Near this threshold, a gap opens up. Probably the most astonishing feature of this spectrum is that, even though the gapless Dirac cone is preserved, the dispersion relation is stretched along the direction perpendicular to the field's polarization. This is an outcome of the electronic dressing and the consequent rescaling of the velocity. This mechanism could be exploited to tune the electronic properties of Dirac materials through the field parameters. A fundamental aspect, yet to be addressed, is the capability of circularly polarized fields to adjust these properties.

V. AUTHOR'S CONTRIBUTIONS

All authors contributed equally to this work.

VI. ACKNOWLEDGEMENTS

This work was supported by DCB UAM-A grant numbers 2232214 and 2232215, and UNAM DGAPA PAPIIT IN102620. J.C.S.S. and V.G.I.S acknowledge the total support from DGAPA-UNAM fellowship.

VII. DATA AVAILABILITY

The data that support the findings of this study are available from the corresponding author upon reasonable request

Appendix A

This Appendix covers the method developed by Whittaker^{56,59} to determine the characteristic exponent (19). Eq. (17) is the starting point. This equation is periodic and therefore its solution must comply with the Floquet theorem. Thus, the solution is given by

$$\chi_\eta(\phi) = e^{i\mu_\eta\phi} u_\eta(\phi), \quad (\text{A1})$$

where $\eta = \pm 1$, $u_\eta(\phi)$ is a function with period π and μ_η denotes the characteristic exponent. Thanks to the periodicity of $u_\eta(\phi)$, the wave function can be expanded as a Fourier series as

$$\chi_\eta(\phi) = e^{i\mu_\eta\phi} \sum_{r=-\infty}^{\infty} C_{2r}^{(\eta)} e^{i2r\phi}. \quad (\text{A2})$$

Substituting the preceding equation into (17) and rearranging the coefficients, we obtain the following recurrence relation

$$\gamma_{2r} C_{2(r-2)}^{(\eta)} + \alpha_{2r} C_{2(r-1)}^{(\eta)} + C_{2r}^{(\eta)} + \beta_{2r} C_{2(r+1)}^{(\eta)} + \gamma_{2r} C_{2(r+2)}^{(\eta)} = 0, \quad (\text{A3})$$

where

$$\alpha_{2r} = \frac{1}{2} \frac{q_1 - i\eta q_3}{a - (\mu + 2r)^2}, \quad (\text{A4})$$

$$\beta_{2r} = \frac{1}{2} \frac{q_1 + i\eta q_3}{a - (\mu + 2r)^2}, \quad (\text{A5})$$

$$\gamma_{2r} = \frac{1}{2} \frac{q_2}{a - (\mu + 2r)^2}. \quad (\text{A6})$$

The equation parameters a , q_1 , q_2 and q_3 are defined in Eqs. (13)-(16). The recurrence relation (A3) can be put in the form of a linear equation as

$$\mathcal{A}_r(\mu, \eta, a, q_1, q_2, q_3) C^{(\eta)} = 0 \quad (\text{A7})$$

where $C^{(\eta)} = (C_2^{(\eta)}, C_4^{(\eta)}, C_6^{(\eta)}, \dots)^\top$ and

$$\mathcal{A}_r(0, \eta, a, q_1, q_2, q_3) = \begin{pmatrix} 1 & \alpha_{2r} & \gamma_{2r} & 0 & 0 & 0 & 0 & 0 & 0 \\ \beta_{2r-2} & \cdot & \cdot & \cdot & \cdot & \cdot & \cdot & \cdot & 0 \\ 0 & \cdot & 1 & \alpha_4 & \gamma_4 & 0 & 0 & \cdot & 0 \\ 0 & \cdot & \beta_2 & 1 & \alpha_2 & \gamma_2 & 0 & \cdot & 0 \\ 0 & \cdot & \gamma_0 & \beta_0 & 1 & \alpha_0 & \gamma_0 & \cdot & 0 \\ 0 & \cdot & 0 & \gamma_{-2} & \beta_{-2} & 1 & \alpha_{-2} & \cdot & 0 \\ 0 & \cdot & 0 & 0 & \gamma_{-4} & \beta_{-4} & 1 & \cdot & 0 \\ 0 & \cdot & \cdot & \cdot & \cdot & \cdot & \cdot & \cdot & \alpha_{-2r+2} \\ 0 & 0 & 0 & 0 & 0 & 0 & \gamma_{-2r} & \beta_{-2r} & 1 \end{pmatrix}. \quad (\text{A8})$$

To avoid the trivial solution we demand that the determinant of the precedent matrix vanishes:

$$\Delta_\eta(0) = \det[\mathcal{A}_r(0, \eta, a, q_1, q_2, q_3)] = 0. \quad (\text{A9})$$

It can be proven that this determinant may be written in the compact form⁵⁹

$$\sin^2\left(\mu_\eta(a) \frac{\pi}{2}\right) = \Delta_\eta(0) \sin^2\left(\sqrt{a} \frac{\pi}{2}\right). \quad (\text{A10})$$

Solving the above equation for $\mu_\eta(a)$ we obtain

$$\mu_\eta(a) = \frac{1}{\pi} \cos^{-1} [1 + \Delta_\eta(0)(\cos(\sqrt{a}\pi) - 1)]. \quad (\text{A11})$$

This expression presents the advantage of being efficiently evaluated by using numerical methods. Strictly speaking \mathcal{A}_r is infinite-dimensional, however good numerical convergence of $\mu_\eta(a)$ is achieved by cutting it down to a 400×400 matrix.

- ¹K. S. Novoselov, V. Fal, L. Colombo, P. Gellert, M. Schwab, K. Kim, *et al.*, “A roadmap for graphene,” *nature* **490**, 192 (2012).
- ²B. Peng, H. Zhang, H. Shao, Y. Xu, R. Zhang, and H. Zhu, “The electronic, optical, and thermodynamic properties of borophene from first-principles calculations,” *Journal of Materials Chemistry C* **4**, 3592–3598 (2016).
- ³T. Wehling, A. M. Black-Schaffer, and A. V. Balatsky, “Dirac materials,” *Advances in Physics* **63**, 1–76 (2014).
- ⁴A. C. Ferrari, F. Bonaccorso, V. Fal’Ko, K. S. Novoselov, S. Roche, P. Bøggild, S. Borini, F. H. Koppens, V. Palermo, N. Pugno, *et al.*, “Science and technology roadmap for graphene, related two-dimensional crystals, and hybrid systems,” *Nanoscale* **7**, 4598–4810 (2015).
- ⁵M. Mehboudi, K. Utt, H. Terrones, E. O. Harriss, A. A. Pacheco San-Juan, and S. Barraza-Lopez, “Strain and the optoelectronic properties of nonplanar phosphorene monolayers,” *Proceedings of the National Academy of Sciences* **112**, 5888–5892 (2015), <https://www.pnas.org/content/112/19/5888.full.pdf>.
- ⁶J. W. Villanova and K. Park, “Spin textures of topological surface states at side surfaces of Bi_2Se_3 from first principles,” *Phys. Rev. B* **93**, 085122 (2016).
- ⁷J. W. Villanova, E. Barnes, and K. Park, “Engineering and probing topological properties of dirac semimetal films by asymmetric charge transfer,” *Nano letters* **17**, 963–972 (2017).
- ⁸F. Bonaccorso, Z. Sun, T. Hasan, and A. Ferrari, “Graphene photonics and optoelectronics,” *Nature photonics* **4**, 611 (2010).
- ⁹Q. Bao, H. Hoh, and Y. Zhang, *Graphene Photonics, Optoelectronics, and Plasmonics* (CRC Press, 2017).
- ¹⁰J. S. Ponraj, Z.-Q. Xu, S. C. Dhanabalan, H. Mu, Y. Wang, J. Yuan, P. Li, S. Thakur, M. Ashrafi, K. Mccoubrey, *et al.*, “Photonics and optoelectronics of two-dimensional materials beyond graphene,” *Nanotechnology* **27**, 462001 (2016).
- ¹¹M. Liu, X. Yin, E. Ulin-Avila, B. Geng, T. Zentgraf, L. Ju, F. Wang, and X. Zhang, “A graphene-based broadband optical modulator,” *Nature* **474**, 64–67 (2011).
- ¹²V. Soriano, M. Midrio, G. Contestabile, I. Asselberghs, J. Van Campenhout, C. Huyghebaert, I. Goykhman, A. Ott, A. Ferrari, and M. Romagnoli, “Graphene–silicon phase modulators with gigahertz bandwidth,” *Nature Photonics* **12**, 40–44 (2018).
- ¹³R. Hao, J. Jiao, X. Peng, Z. Zhen, R. Dagarbek, Y. Zou, and E. Li, “Experimental demonstration of a graphene-based hybrid plasmonic modulator,” *Optics letters* **44**, 2586–2589 (2019).
- ¹⁴Z. Yin, J. Zhu, Q. He, X. Cao, C. Tan, H. Chen, Q. Yan, and H. Zhang, “Graphene-based materials for solar cell applications,” *Advanced energy materials* **4**, 1300574 (2014).
- ¹⁵P. O’keeffe, D. Catone, A. Paladini, F. Toschi, S. Turchini, L. Avaldi, F. Martelli, A. Agresti, S. Pescetelli, A. Del Rio Castillo, *et al.*, “Graphene-induced improvements of perovskite solar cell stability: Effects on hot-carriers,” *Nano letters* **19**, 684–691 (2019).
- ¹⁶A. Safaei, S. Chandra, M. W. Shabbir, M. N. Leuenberger, and D. Chanda, “Dirac plasmon-assisted asymmetric hot carrier generation for room-temperature infrared detection,” *Nature communications* **10**, 1–7 (2019).
- ¹⁷A. Grigorenko, M. Polini, and K. Novoselov, “Graphene plasmonics,” *Nature photonics* **6**, 749 (2012).
- ¹⁸Y. Fan, N.-H. Shen, F. Zhang, Q. Zhao, H. Wu, Q. Fu, Z. Wei, H. Li, and C. M. Soukoulis, “Graphene plasmonics: a platform for 2d optics,” *Advanced Optical Materials* **7**, 1800537 (2019).
- ¹⁹F. J. Lopez-Rodríguez and G. G. Naumis, “Analytic solution for electrons and holes in graphene under electromagnetic waves: Gap appearance and nonlinear effects,” *Phys. Rev. B* **78**, 201406(R) (2008).
- ²⁰F. López-Rodríguez and G. Naumis, “Graphene under perpendicular incidence of electromagnetic waves: Gaps and band structure,” *Philosophical Magazine* **90**, 2977–2988 (2010).
- ²¹O. V. Kibis, “Metal-insulator transition in graphene induced by circularly polarized photons,” *Phys. Rev. B* **81**, 165433 (2010).
- ²²H. L. Calvo, H. M. Pastawski, S. Roche, and L. E. F. F. Torres, “Tuning laser-induced band gaps in graphene,” *Applied Physics Letters* **98**, 232103 (2011), <https://doi.org/10.1063/1.3597412>.
- ²³D. Sun, G. Aivazian, A. M. Jones, J. S. Ross, W. Yao, D. Cobden, and X. Xu, “Ultrafast hot-carrier-dominated photocurrent in graphene,” *Nature nanotechnology* **7**, 114 (2012).
- ²⁴K. Kristinsson, O. V. Kibis, S. Morina, and I. A. Shelykh, “Control of electronic transport in graphene by electromagnetic dressing,” *Scientific Reports* **6**, 20082 EP – (2016).
- ²⁵K. Kristinsson, O. V. Kibis, S. Morina, and I. A. Shelykh, “Control of electronic transport in graphene by electromagnetic dressing,” *Scientific reports* **6**, 1–7 (2016).
- ²⁶O. Kibis, K. Dini, I. Iorsh, and I. Shelykh, “All-optical band engineering of gapped dirac materials,” *Physical Review B* **95**, 125401 (2017).
- ²⁷O. Kibis, K. Dini, I. Iorsh, V. Dragunov, and I. Shelykh, “Electromagnetic dressing of graphene,” *Journal of Structural Chemistry* **59**, 867–869 (2018).
- ²⁸C.-K. Chan, N. H. Lindner, G. Refael, and P. A. Lee, “Photocurrents in weyl semimetals,” *Phys. Rev. B* **95**, 041104 (2017).
- ²⁹G. G. Naumis, S. Barraza-Lopez, M. Oliva-Leyva, and H. Terrones, “Electronic and optical properties of strained graphene and other strained 2d materials: a review,” *Reports on Progress in Physics* **80**, 096501 (2017).
- ³⁰R. Carrillo-Bastos and G. G. Naumis, “Band gaps and wavefunctions of electrons coupled to pseudo electromagnetic waves in rippled graphene,” *physica status solidi (RRL)–Rapid Research Letters* **12**, 1800072 (2018).
- ³¹T. Higuchi, C. Heide, K. Ullmann, H. B. Weber, and P. Hommelhoff, “Light-field-driven currents in graphene,” *Nature* **550**, 224–228 (2017).
- ³²E. G. Mishchenko, “Effect of electron-electron interactions on the conductivity of clean graphene,” *Phys. Rev. Lett.* **98**, 216801 (2007).
- ³³S. A. Herrera and G. G. Naumis, “Electronic and optical conductivity of kekul’e-patterned graphene: Intravalley and intervalley transport,” *arXiv preprint arXiv:2001.07195* (2020).
- ³⁴B. Mielnik and D. J. Fernández C., “An electron trapped in a rotating magnetic field,” *Journal of Mathematical Physics* **30**, 537–549 (1989), <https://doi.org/10.1063/1.528419>.
- ³⁵B. Mielnik and C. David J. Fernández, “Is there an instability transition in standing wave traps?” *Letters in Mathematical Physics* **17**, 87–94 (1989).
- ³⁶M. Goerbig, J.-N. Fuchs, G. Montambaux, and F. Piéchon, “Tilted anisotropic dirac cones in quinoid-type graphene and α -(bedt-ttf) 2 i 3,” *Physical Review B* **78**, 045415 (2008).
- ³⁷B. Feng, J. Zhang, S. Ito, M. Arita, C. Cheng, L. Chen, K. Wu, F. Komori, O. Sugino, K. Miyamoto, T. Okuda, S. Meng, and I. Matsuda, “Discovery of 2d anisotropic dirac cones,” *Advanced Materials* **30**, 1704025 (2018), <https://onlinelibrary.wiley.com/doi/pdf/10.1002/adma.201704025>.
- ³⁸M. Mehboudi, A. M. Dorio, W. Zhu, A. van der Zande, H. O. Churchill, A. A. Pacheco-Sanjuan, E. O. Harriss, P. Kumar, and S. Barraza-Lopez, “Two-dimensional disorder in black phosphorus and monochalcogenide monolayers,” *Nano letters* **16**, 1704–1712 (2016).
- ³⁹K. L. Utt, P. Rivero, M. Mehboudi, E. O. Harriss, M. F. Borunda, A. A. Pacheco SanJuan, and S. Barraza-Lopez, “Intrinsic defects, fluctuations of the local shape, and the photo-oxidation of black phosphorus,” *ACS central science* **1**, 320–327 (2015).
- ⁴⁰S. P. Poudel, J. W. Villanova, and S. Barraza-Lopez, “Group-iv monochalcogenide monolayers: Two-dimensional ferroelectrics with weak intralayer bonds and a phosphorene like monolayer dissociation energy,” *Phys. Rev. Materials* **3**, 124004 (2019).
- ⁴¹S. W. Jung, S. H. Ryu, W. J. Shin, Y. Sohn, M. Huh, R. J. Koch, C. Jozwiak, E. Rotenberg, A. Bostwick, and K. S. Kim, “Black phosphorus as a bipolar pseudospin semiconductor,” *Nature Materials* (2020), [10.1038/s41563-019-0590-2](https://doi.org/10.1038/s41563-019-0590-2).
- ⁴²S. Verma, A. Mawrie, and T. K. Ghosh, “Effect of electron-hole asymmetry on optical conductivity in 8-pmmn borophene,” *Physical Review B* **96**, 155418 (2017).
- ⁴³A. E. Champo and G. G. Naumis, “Metal-insulator transition in 8-Pmmn borophene under normal incidence of electromagnetic radiation,” *Physical Review B* **99**, 1–7 (2019).
- ⁴⁴I. Boustani, “New quasi-planar surfaces of bare boron,” *Surface Science* **370**, 355 – 363 (1997).
- ⁴⁵Z. Zhang, E. S. Penev, and B. I. Yakobson, “Two-dimensional boron: structures, properties and applications,” *Chemical Society Reviews* **46**, 6746–6763 (2017).
- ⁴⁶A. J. Mannix, Z. Zhang, N. P. Guisinger, B. I. Yakobson, and M. C. Hersam, “Borophene as a prototype for synthetic 2d materials development,” *Nature nanotechnology* **13**, 444–450 (2018).
- ⁴⁷A. D. Zabolotskiy and Y. E. Lozovik, “Strain-induced pseudomagnetic field in the Dirac semimetal borophene,” *Physical Review B* **94**, 1–6 (2016).

- ⁴⁸V. Ibarra-Sierra, J. Sandoval-Santana, A. Kunold, and G. G. Naumis, “Dynamical band gap tuning in anisotropic tilted dirac semimetals by intense elliptically polarized normal illumination and its application to 8-*p m m n* borophene,” *Physical Review B* **100**, 125302 (2019).
- ⁴⁹T. Dittrich, P. Hänggi, G.-L. Ingold, B. Kramer, G. Schön, and W. Zwerger, *Quantum transport and dissipation*, Vol. 3 (Wiley-Vch Weinheim, 1998).
- ⁵⁰C. D. J. Fernandez, M. A. del Olmo, and M. Santander, “Orbital aharonov-anandan geometric phase for confined motion in a precessing magnetic field,” *Journal of Physics A: Mathematical and General* **25**, 6409–6418 (1992).
- ⁵¹S. C. y Cruz and B. Mielnik, “Non-inertial quantization: Truth or illusion?” in *Journal of Physics: Conference Series*, Vol. 698 (IOP Publishing, 2016) p. 012002.
- ⁵²H. Hübener, M. A. Sentef, U. De Giovannini, A. F. Kemper, and A. Rubio, “Creating stable floquet–weyl semimetals by laser-driving of 3d dirac materials,” *Nature communications* **8**, 1–8 (2017).
- ⁵³T. Oka and S. Kitamura, “Floquet engineering of quantum materials,” *Annual Review of Condensed Matter Physics* **10**, 387–408 (2019), <https://doi.org/10.1146/annurev-conmatphys-031218-013423>.
- ⁵⁴S. A. Herrera and G. G. Naumis, “Kubo conductivity for anisotropic tilted dirac semimetals and its application to 8-*pmmn* borophene: Role of frequency, temperature, and scattering limits,” *Phys. Rev. B* **100**, 195420 (2019).
- ⁵⁵B. Dey and T. K. Ghosh, “Photoinduced valley and electron-hole symmetry breaking in α -t 3 lattice: The role of a variable berry phase,” *Physical Review B* **98**, 075422 (2018).
- ⁵⁶W. Magnus and S. Winkler, *Hill’s equation* (Courier Corporation, 2013).
- ⁵⁷K. M. Urwin and F. Arscott, “Iii.—theory of the whittaker hill equation,” *Proceedings of the Royal Society of Edinburgh Section A: Mathematics* **69**, 28–44 (1970).
- ⁵⁸C. Ziener, M. Rückl, T. Kampf, W. Bauer, and H. Schlemmer, “Mathieu functions for purely imaginary parameters,” *Journal of Computational and Applied Mathematics* **236**, 4513 – 4524 (2012).
- ⁵⁹J. Lachapelle and R. H. Brandenberger, “Preheating with non-standard kinetic term,” *Journal of Cosmology and Astroparticle Physics* **2009**, 020–020 (2009).
- ⁶⁰Y. Zhou and M. W. Wu, “Optical response of graphene under intense terahertz fields,” *Phys. Rev. B* **83**, 245436 (2011).
- ⁶¹M. Bukov, L. D’Alessio, and A. Polkovnikov, “Universal high-frequency behavior of periodically driven systems: from dynamical stabilization to floquet engineering,” *Adv. Phys.* **64**, 139–226 (2015).
- ⁶²V. Gritsev and A. Polkovnikov, “Integrable floquet dynamics,” *SciPost Phys.* **2**, 021 (2017).
- ⁶³J. C. Sandoval-Santana, V. G. Ibarra-Sierra, J. L. Cardoso, A. Kunold, P. Roman-Taboada, and G. Naumis, “Method for finding the exact effective hamiltonian of time-driven quantum systems,” *Annalen der Physik* **531**, 1900035 (2019).